Article

Cell Reports

The NAD+ Precursor Nicotinamide Riboside Rescues Mitochondrial Defects and Neuronal Loss in iPSC and Fly Models of Parkinson's Disease

Graphical Abstract

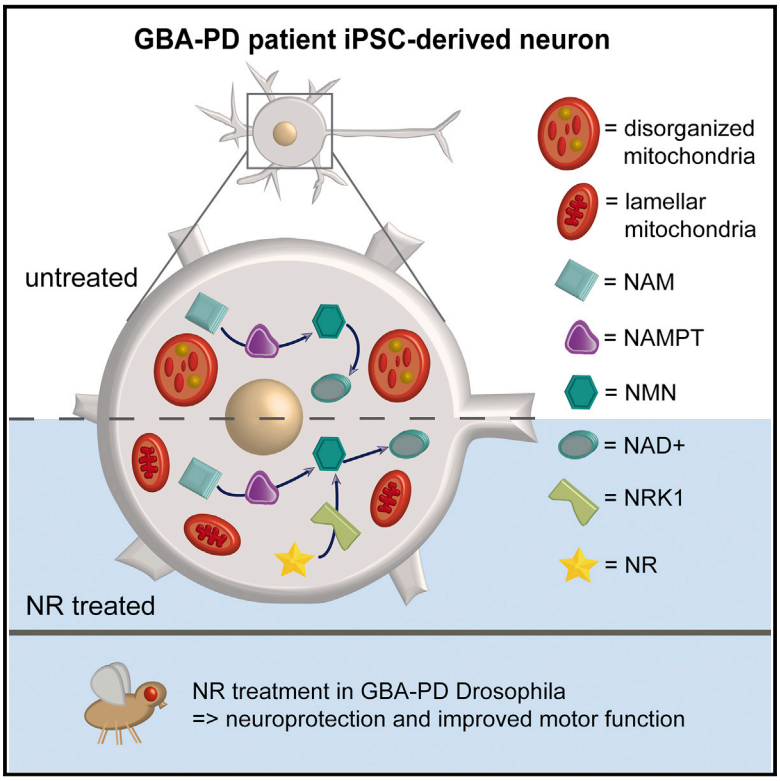

Highlights

- NAD+ metabolism and mitochondrial function are altered in GBA-PD neurons
- Human iPSC-derived neurons are responsive to NAD+ precursors
- Nicotinamide riboside improves mitochondrial function in GBA-PD iPSC neurons
- Nicotinamide riboside rescues neuronal loss and motor deficits in GBA-PD flies

Authors

David C. Schöndorf, Dina Ivanyuk, Pascale Baden, ..., Thomas Gasser, Alexander J. Whitworth, Michela Deleidi

Correspondence

michela.deleidi@dzne.de

In Brief

Mitochondrial damage is a key feature in Parkinson's disease. Schöndorf et al. demonstrate that nicotinamide riboside, an NAD+ precursor, boosts mitochondrial function in neurons derived from Parkinson's disease patient stem cells and is neuroprotective in Parkinson's disease fly models. These findings support use of NAD+ precursors in Parkinson's and other neurodegenerative diseases.

Schöndorf et al., 2018, Cell Reports *23*, 2976–2988
June 5, 2018
https://doi.org/10.1016/j.celrep.2018.05.009

CellPress

OPEN ACCESS
CellPress

Cell Reports
Article

The NAD+ Precursor Nicotinamide Riboside Rescues Mitochondrial Defects and Neuronal Loss in iPSC and Fly Models of Parkinson's Disease

David C. Schöndorf,[1,2] Dina Ivanyuk,[1,2,8] Pascale Baden,[1,2,8] Alvaro Sanchez-Martinez,[3] Silvia De Cicco,[1,2] Cong Yu,[1,2] Ivana Giunta,[3] Lukas K. Schwarz,[1,2] Gabriele Di Napoli,[1,2] Vasiliki Panagiotakopoulou,[1,2] Sigrun Nestel,[4] Marcus Keatinge,[5] Jan Pruszak,[6,7] Oliver Bandmann,[5] Bernd Heimrich,[4] Thomas Gasser,[1,2] Alexander J. Whitworth,[3] and Michela Deleidi[1,2,9,*]

[1]German Center for Neurodegenerative Diseases (DZNE), Helmholtz Association, Tübingen 72076, Germany
[2]Hertie-Institute for Clinical Brain Research, University of Tübingen, Tübingen 72076, Germany
[3]Medical Research Council Mitochondrial Biology Unit, University of Cambridge, Cambridge Biomedical Campus, Hills Road, Cambridge CB2 0XY, UK
[4]Department of Neuroanatomy, Institute of Anatomy and Cell Biology, University of Freiburg, Freiburg 79104, Germany
[5]Sheffield Institute for Translational Neuroscience (SITraN), University of Sheffield, Sheffield, UK
[6]Emmy Noether-Group for Stem Cell Biology, Department of Molecular Embryology, Institute of Anatomy and Cell Biology, Faculty of Medicine, University of Freiburg, Freiburg, Germany
[7]Center for Biological Signaling Studies (BIOSS), University of Freiburg, Freiburg 79104, Germany
[8]These authors contributed equally
[9]Lead Contact
*Correspondence: michela.deleidi@dzne.de
https://doi.org/10.1016/j.celrep.2018.05.009

SUMMARY

While mitochondrial dysfunction is emerging as key in Parkinson's disease (PD), a central question remains whether mitochondria are actual disease drivers and whether boosting mitochondrial biogenesis and function ameliorates pathology. We address these questions using patient-derived induced pluripotent stem cells and *Drosophila* models of *GBA*-related PD (*GBA*-PD), the most common PD genetic risk. Patient neurons display stress responses, mitochondrial demise, and changes in NAD+ metabolism. NAD+ precursors have been proposed to ameliorate age-related metabolic decline and disease. We report that increasing NAD+ via the NAD+ precursor nicotinamide riboside (NR) significantly ameliorates mitochondrial function in patient neurons. Human neurons require nicotinamide phosphoribosyltransferase (NAMPT) to maintain the NAD+ pool and utilize NRK1 to synthesize NAD+ from NAD+ precursors. Remarkably, NR prevents the age-related dopaminergic neuronal loss and motor decline in fly models of *GBA*-PD. Our findings suggest NR as a viable clinical avenue for neuroprotection in PD and other neurodegenerative diseases.

INTRODUCTION

Mitochondrial dysfunction has been proposed as a key mechanism in many neurodegenerative diseases. Among others, Parkinson's disease (PD) stands out due to the role of PD-linked genes in mitochondrial function and dynamics (Exner et al., 2012). Evidence for mitochondrial dysfunction in PD was first described in the 1980s by Schapira et al., who showed complex I (CI) defects in cells and tissues from PD patients (Schapira et al., 1989). Substantial progress has been made since, and genetic and biochemical studies now indicate that mitochondrial dysfunction and cellular energy failure are key to PD (Jansen et al., 2017). In this respect, recent studies have shown that the activation of pathways related to mitochondrial biogenesis and energy metabolism, such as the NAD+/sirtuin 1 (SIRT1) pathway, provides protection against aging-related disease (Rajman et al., 2018). Similar approaches could be easily translated into treatment for PD. However, it is still unclear whether mitochondrial defects are actual disease drivers and increasing mitochondrial biogenesis provides neuroprotection in PD. In addition, little is known about NAD+ metabolism and availability of NAD+ precursors in human neurons. Here, we have addressed these fundamental questions in an induced pluripotent stem cell (iPSC) neuronal model of PD bearing mutations in the lysosomal enzyme β-Glucocerebrosidase (*GBA*) gene (*GBA*-PD), the most common genetic risk for PD (Sidransky et al., 2009). β-Glucocerebrosidase (GCase) activity is reduced not only in mutation carriers but also in idiopathic PD and healthy individuals at older age (Gegg et al., 2012; Rocha et al., 2015), pointing toward a general role for GCase in brain aging and neurodegenerative processes. Importantly, patients with *GBA* mutations represent an etiologically homogeneous subgroup of PD, therefore providing the ideal cohort for precision medicine approaches.

The pathogenetic mechanisms involved in *GBA*-PD are only partially understood and include autophagic defects, increased α-synuclein aggregation, calcium dyshomeostasis,

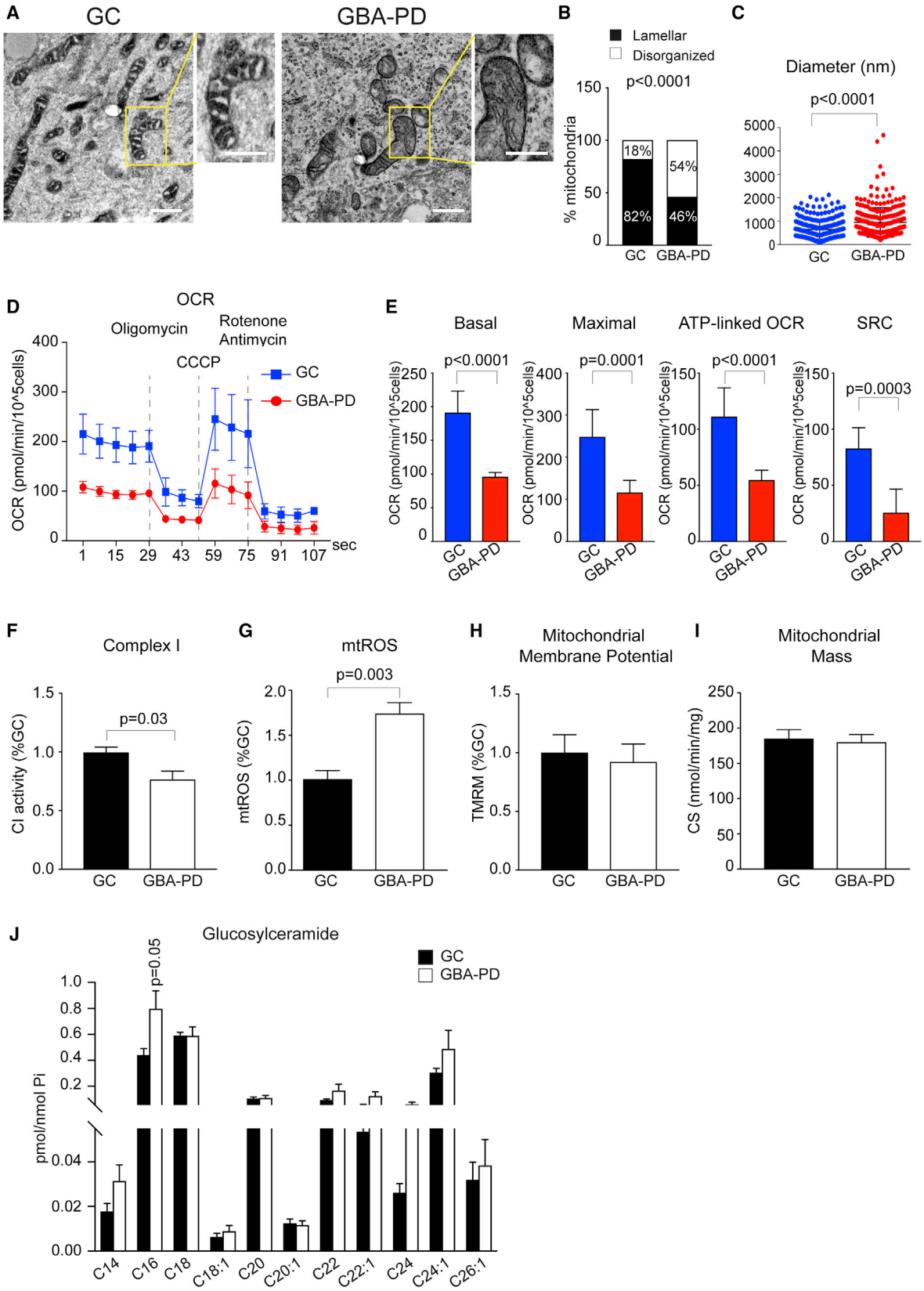

(legend on next page)

and endoplasmic reticulum (ER) stress (Migdalska-Richards and Schapira, 2016). GCase is a lysosomal enzyme that catalyzes the hydrolysis of glucosylceramide (GlcCer), a membrane glycosphingolipid, to ceramide and glucose, and both loss and gain of its enzymatic function may contribute to disease. According to the loss-of-function hypothesis, GCase deficiency causes substrate accumulation that alters lysosomal function and promotes α-synuclein aggregation (Jo et al., 2000; Velayati et al., 2010; Mazzulli et al., 2011). GCase is glycosylated and folded in the ER and subsequently trafficked through the Golgi to the lysosome. According to the gain-of-function hypothesis, *GBA* mutations interfere with the folding process in the ER, leading to ER-associated degradation, ER stress, and activation of the unfolded protein response (UPR) (Maor et al., 2013; Fernandes et al., 2016). Interestingly, mitochondrial dysfunction has been described in experimental models of GCase deficiency (Osellame et al., 2013; Keatinge et al., 2015; Cleeter et al., 2013). However, whether mitochondrial function is altered in PD patients with *GBA* mutations (*GBA*-PD) and the mechanisms underlying such demise are still unknown. Furthermore, whether improving mitochondrial biogenesis and function represents an effective therapeutic strategy for PD needs to be investigated.

RESULTS

iPSC-Derived Neurons from *GBA*-PD Patients Show Defects in Mitochondrial Function

To investigate whether *GBA* is linked to mitochondrial function in human neurons, iPSC lines from PD patients with heterozygous *GBA* mutations (N370S, L444P, and RecNcil), as well as corresponding isogenic gene-corrected (GC) and unaffected controls (Schöndorf et al., 2014) (Table S1), were differentiated into dopaminergic (DA) neurons, and mitochondrial morphology was examined by transmission electron microscopy (TEM). Morphometric analysis revealed altered cristae morphology in *GBA*-PD neurons compared to isogenic GC and healthy controls (Figures 1A, 1B, and S1A). In addition, *GBA*-PD neurons showed a significant increase in mitochondrial diameter (Figure 1C). Next, we measured oxygen consumption rates (OCRs) and found that *GBA*-PD neurons displayed significantly reduced basal respiration and decreased maximal OCR as well as ATP-linked OCR and spare respiratory capacity (SRC) compared to isogenic controls (Figures 1D and 1E). Similarly, basal respiration, maximal OCR, and ATP-linked OCR and SRC were significantly reduced in *GBA*-PD neurons compared to unrelated unaffected controls (Figure S1B). Western blot analysis revealed an increase in the level of respiratory chain complex subunits in *GBA*-PD neurons compared to isogenic controls, but this increase did not reach statistical significance (Figures S1C and S1D). We next measured CI activity in enriched mitochondrial fractions from *GBA*-PD iPSC neurons and GC controls. CI activity was significantly reduced in *GBA*-PD neurons compared to isogenic controls (Figure 1F). Consistent with these findings, *GBA*-PD neurons produced significantly higher amounts of mitochondrial reactive oxygen species (mtROS) than isogenic controls (Figure 1G). However, mitochondrial membrane potential and mitochondrial mass were not significantly changed in *GBA*-PD neurons (Figures 1H and 1I). Of note, no significant difference in the degree of mitochondrial function was observed among different *GBA* genotypes, suggesting that the genotypes examined in this study (RecNcil, L444P, and N370S) equally affect mitochondria (Figures S1E–S1I). To get further insight into the mechanisms underlying mitochondrial dysfunction in *GBA*-PD, we examined the GCase substrate sphingolipid composition of mitochondria from *GBA*-PD neurons and isogenic controls by high-performance liquid chromatography tandem mass spectrometry (HPLC-MS/MS). To this end, mitochondria were isolated from iPSC neurons with a high degree of purity. Western blot analysis showed high level of enrichment of isolated mitochondria with a small amount of non-mitochondrial organelle contamination (Figure S1J). Quantification of individual species of GlcCer revealed the absence of GlcCer accumulation in patient mitochondria with only a significant increase of C16-GlcCer (Figure 1J).

iPSC-Derived Neurons from *GBA*-PD Patients Show Defects in Mitochondrial Dynamics

Next, we examined the level of mitochondrial fission (DRP1 and Fis1) and fusion (OPA1 and Mfn1) proteins in *GBA*-PD iPSC neurons and isogenic controls. Immunoblot analysis revealed a

Figure 1. Mitochondrial Function in *GBA*-PD iPSC Neurons

(A–C) Mitochondrial morphology in isogenic gene-corrected (GC) controls and *GBA*-PD iPSC neurons.

(A) Representative TEM images of mitochondria are shown (L444P *GBA*-PD and GC controls) (scale bar, 500 nm).

(B) Quantification of mitochondrial cristae morphology in isogenic GC and *GBA*-PD (N370S, L444P) iPSC-derived neurons (n = 3; two-sided Fisher's exact test).

(C) Mitochondrial major diameter. Data are presented as mean ± SD (n = 299 GC and n = 264 *GBA*-PD mitochondria from 3 independent experiments were analyzed; two-tailed t test).

(D) Oxygen consumption rate (OCR) trace for isogenic GC and *GBA*-PD (N370S, L444P, RecNcil) iPSC neurons. Data are normalized to cell number and presented as mean ± SD (n = 8; two-tailed t test).

(E) Quantification of basal, maximal, ATP-linked respiration, and spare respiratory capacity (SRC). Data are normalized to cell number and presented as mean + SD (n = 8; two-tailed t test).

(F) Complex I (CI) activity in enriched mitochondria from isogenic *GBA*-PD (N370S, L444P) and GC iPSC neurons. Data are expressed as mean + SEM (n = 5; two-tailed t test).

(G) Mitochondrial ROS (mtROS) levels in *GBA*-PD (N370S, L444P, RecNcil) and GC iPSC neurons. Data are normalized to GC and represented as mean + SEM (n = 5; two-tailed t test).

(H) Mitochondrial membrane potential in isogenic GC and *GBA*-PD (N370S, L444P, RecNcil) iPSC neurons. Data are normalized to GC and presented as mean + SEM (n = 5; two-tailed t test).

(I) Citrate synthase (CS) activities in GC and *GBA*-PD (N370S, L444P, RecNcil) iPSC neurons. Data are presented as mean + SEM (n = 5; two-tailed t test).

(J) Mitochondrial sphingolipid profile of isogenic GC and *GBA*-PD (N370S, L444P) iPSC neurons. Data are normalized to inorganic phosphate (Pi) and presented as mean + SEM (n = 7 independent mitochondrial purifications; two-tailed t test).

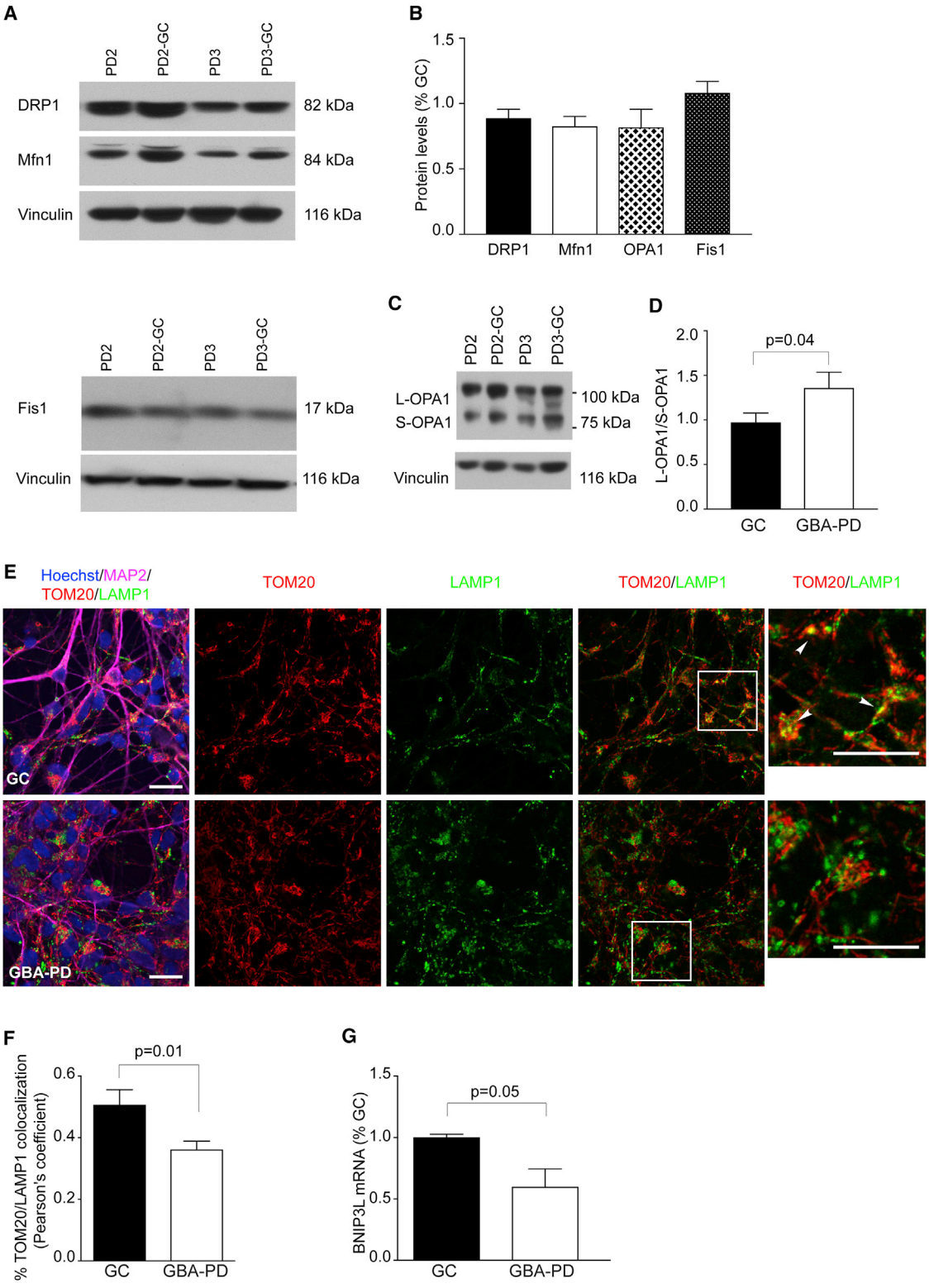

Figure 2. Mitochondrial Dynamics in *GBA*-PD iPSC Neurons

(A and B) Western blot of DRP1, Mfn1, and Fis1 in isogenic *GBA*-PD (N370S, L444P) and gene-corrected (GC) iPSC neurons (A). Vinculin was used as a loading control. Quantification of western blots is shown in (B). Data are normalized to GC and presented as mean + SEM (n = 5).

(C and D) Western blot analysis of OPA-1 processing (C). The L-OPA1/S-OPA-1 ratio is shown in (D). Data are presented as mean + SEM (n = 5; two-tailed t test).

(legend continued on next page)

reduction in DRP1, OPA1, and Mfn1 levels in *GBA*-PD neurons (Figures 2A–2D). On the other hand, there was an increase of Fis1 in *GBA*-PD neurons (Figures 2A and 2B). However, these differences did not reach statistical significance. Interestingly, the ratio between the long and short form of OPA1 was significantly increased in *GBA*-PD neurons compared to isogenic controls, suggesting an impairment of mitophagy (MacVicar and Lane, 2014) (Figures 2C and 2D). *GBA*-PD neurons showed a significant reduction of mitochondrial-lysosomal co-localization compared to GC controls, as assessed by confocal microscopy and Amnis ImageStream flow cytometry (Figures 2E, 2F, S2A, and S2B). In line with these findings, the expression of the mitophagy adaptor protein BNIP3L/NIX was significantly reduced in *GBA*-PD compared to isogenic controls (Figure 2G).

Mitochondrial Function Is Altered in *GBA* Knockout iPSC-Derived Neurons

To assess the impact of loss of GCase enzymatic function on mitochondria in the absence of gain-of-function mechanisms, we generated *GBA* knockout (KO) iPSCs using clustered regularly interspaced short palindromic repeats (CRISPR)-Cas9 (Figures S3A–S3F). *GBA* was knocked out in two healthy control iPSC lines and one *GBA-PD* N370S iPSC line (Table S2). All *GBA* KO clones showed complete loss of GCase protein and its enzymatic activity (Figures S3E and S3F). No significant difference in DA neuronal differentiation potential was observed among *GBA* KO iPSCs and corresponding parental lines as assessed by quantification of βIII-tubulin- and tyrosine hydroxylase (TH)-positive neurons (>80% neurons, of which on average 40% of cells in both controls and *GBA* KO lines expressed TH). *GBA* KO iPSC-derived neurons exhibited accumulation of the GCase substrates GlcCer and glucosylsphingosine as revealed by HPLC-MS/MS (Figures S3G). A significant increase of C16-galactosylceramide was also observed (Figure S3I). No significant change in levels of other sphingolipids was detected (Figures S3H and S3I). Two *GBA* KO clones were selected from each parental iPSC line and used for further experiments (Table S2). As observed in *GBA*-PD neurons, morphometric analysis revealed ultrastructural abnormalities in *GBA* KO iPSC-neurons compared to isogenic controls (Figures 3A and 3B). Similar to what we observed in *GBA*-PD neurons, *GBA* KO neurons showed significantly reduced basal and maximal respiration as well as ATP-linked OCR and SRC (Figure 3C). Despite the consistent trend for decreased CI activity in *GBA* KO neurons, the values did not reach statistical significance (Figure 3D). *GBA* KO neurons showed elevated levels of mtROS (Figure 3E). Furthermore, we did not observe significant changes of mitochondrial membrane potential (Figure 3F). HPLC-MS/MS analysis of mitochondria purified from *GBA* KO iPSC-derived neurons showed a significant accumulation of all subtypes of the GCase substrates GlcCer and glucosylsphingosine (Figure 3G).

GBA-PD, but Not *GBA* Knockout, iPSC-Derived Neurons Show Increased ER Stress and UPR

Interestingly, when comparing OCRs and CI activity in the isogenic lines (*GBA*-PD N370S, GC control and *GBA* KO), no gene dosage effect was found (Figures S3J and S3K). These data suggest that different mechanisms contribute to mitochondrial defects in heterozygous *GBA*-PD patient and *GBA* KO neurons. One of such mechanisms could be the UPR and ER stress that have been previously observed in *GBA-PD* (Fernandes et al., 2016). To dissect the contribution of gain- and loss-of-function of mutant GCase, we measured the levels of the ER chaperone immunoglobulin-binding protein (BiP) by western blot in *GBA*-PD N370S iPSC-derived neurons as well as isogenic controls and isogenic *GBA* KO neurons. Levels of BiP were increased in *GBA*-PD neurons compared to isogenic controls and isogenic *GBA* KO neurons (Figure 4A). Consistent with these findings, RNA levels of spliced X-box-binding protein-1 (XBP1s) were significantly increased in *GBA*-PD, but not in isogenic *GBA* KO neurons, suggesting activation of the IRE1 related branch of ER stress (Figure 4B). Healthy control-derived *GBA* KO neurons showed levels of BiP similar to their isogenic controls (Figure S3L). In addition, levels of phospho-eIF2α were significantly increased in *GBA*-PD, but not in isogenic *GBA* KO neurons, as compared to GC controls (Figure 4C). Consistent with these findings, levels of phospho-PERK were increased only in *GBA*-PD neurons as compared to GC controls (Figure 4D).

NAD+ Metabolism Is Altered in *GBA*-PD iPSC-Derived Neurons

Mitochondrial dysfunction and increased oxidative stress are hallmarks of aging and have been linked to the decline of intracellular levels of NAD+ (Mouchiroud et al., 2013). To examine whether *GBA* mutations lead to changes in NAD+ metabolism, we measured the expression of the NAD+ biosynthetic enzymes nicotinamide mononucleotide adenylyltransferases (NMNATs). mRNA levels of NMNAT2 were significantly decreased in *GBA*-PD neurons compared to isogenic controls, whereas levels of NMNAT1 and NMNAT3 were unchanged (Figure 5A). NMNAT2 levels were unchanged in *GBA* KO neurons (Figure S3M). Levels of nicotinamide phosphoribosyltransferase (NAMPT), the rate-limiting enzyme in the NAD+ salvage synthesis pathway, were similar in both groups (*GBA*-PD and GC controls), as assessed by qRT-PCR (Figure 5A). Next, we measured the adenine and pyridine nucleotide pool in *GBA*-PD and isogenic control as well as *GBA* KO iPSC-neurons by targeted metabolomics using liquid chromatography-mass spectrometry (LC-MS). The intracellular NAD+ content was maintained in *GBA*-PD and *GBA* KO neurons (Figure S4). To exclude that the observed absence of significant changes of NAD+ levels could be linked to the absence of overt neurodegeneration in our stem cell-based model system, we also examined the NAD+ metabolome in adult *gba*$^{+/+}$, *gba*$^{-/-}$, and gba$^{+/-}$ whole zebrafish brains. Adult *gba*$^{-/-}$

(E) Immunostaining of differentiated iPSC cultures for MAP2 (magenta), TOM20 (red), and LAMP1 (green). Cell nuclei were counterstained with Hoechst (blue). Scale bar, 20 μm.

(F) Colocalization between LAMP1 and TOM20. Data are presented as mean + SEM (n = 5; two-tailed t test).

(G) BNIP3L mRNA levels in isogenic GC and *GBA*-PD (N370S, L444P) iPSC-derived neurons. Data are normalized on Rplp0 and OAZ1 and to GC and presented as mean + SEM (n = 5; two-tailed t test).

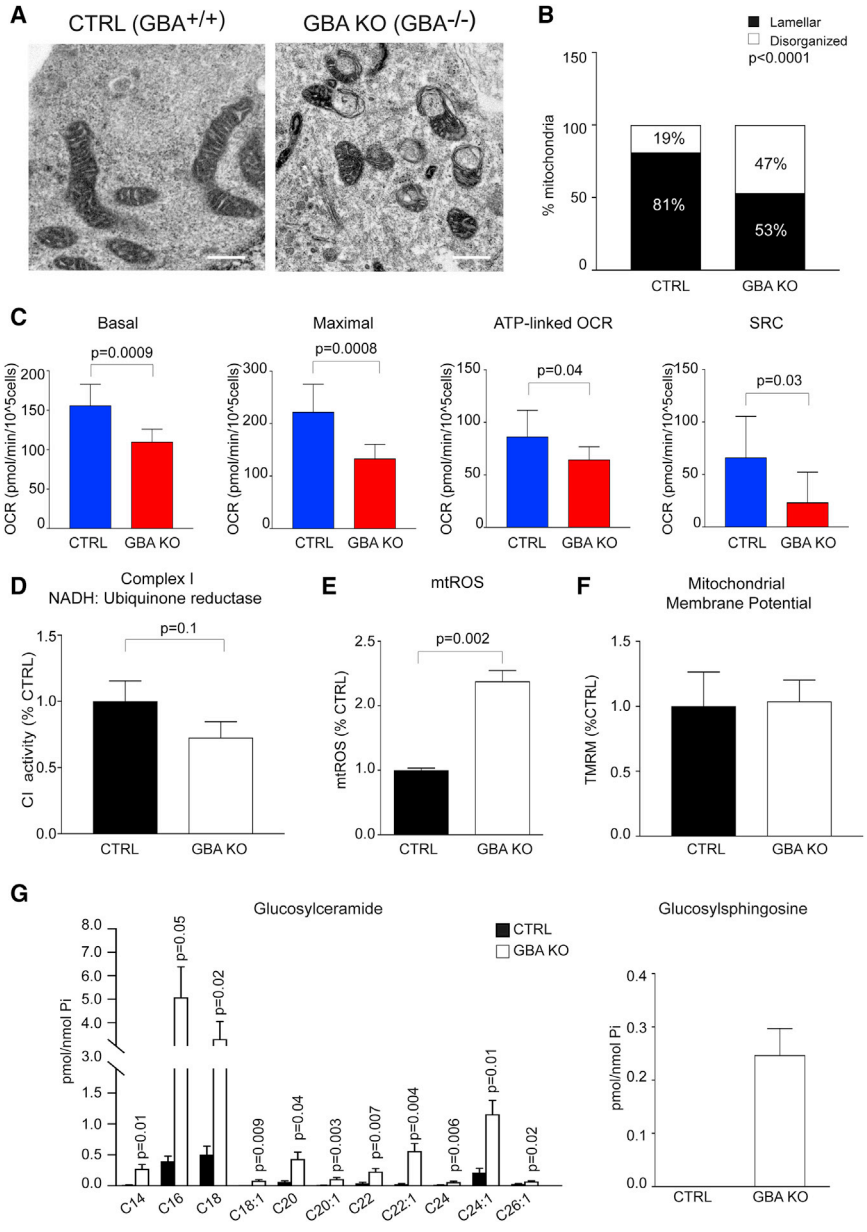

Figure 3. Mitochondrial Function in Human *GBA* KO iPSC Neurons

(A and B) Mitochondrial morphology in isogenic healthy control (CTRL) and *GBA* KO iPSC neurons. Representative TEM images of mitochondria (A; scale bar, 500 nm). Quantification of mitochondrial cristae morphology in isogenic CTRL and *GBA* KO iPSC-neurons (B). Data are presented as mean + SEM (n = 3; two-sided Fisher's exact test).

(C) Mitochondrial respiration. Data are presented as mean + SD (n = 5–7; two-tailed t test).

(D) CI activity in isogenic CTRL and *GBA* KO iPSC neurons. Data are expressed as mean + SEM (n = 5; two-tailed t test).

(E) mtROS levels normalized to CTRL and presented as mean + SEM (n = 5; two-tailed t test).

(F) Mitochondrial membrane potential. Data are presented as mean + SEM (n = 5; two-tailed t test).

(G) Mitochondrial sphingolipid profile of CTRL and *GBA* KO iPSC-neurons. GlcCer and glucosylsphingosine levels normalized by inorganic phosphate (Pi). Glucosylsphingosine was below detection limit in control mitochondria. Data are presented as mean + SEM (n = 4 independent mitochondrial purifications; two-tailed t test).

zebrafish recapitulate the key pathological aspects of PD, including DA neuronal loss, early microglial activation, and mitochondrial dysfunction (Keatinge et al., 2015). Metabolomic analyses revealed that the NAD+ pool was maintained in brains of adult *gba*$^{+/-}$ and *gba*$^{-/-}$ zebrafish (Figure S5). However, a significant increase in nicotinamide mononucleotide (NMN) was observed in *gba*$^{-/-}$ compared to *gba*$^{+/+}$ zebrafish brains as well as in *gba*$^{-/-}$ compared to *gba*$^{+/-}$ brains (Figure S5), suggesting an alteration of NAD+ metabolism. To rule out the possibility that the heterogeneity of the cell culture and whole brain tissues influences the results, we then employed the biosensor Peredox to monitor the cytosolic NADH/NAD+ ratio in single iPSC-derived neurons with live-cell imaging (Hung et al., 2011). The NAD+/NADH redox state was significantly reduced in *GBA*-PD iPSC neurons, suggesting reduced level of available NAD+ (Figure 5B). No significant change was observed in *GBA* KO neurons (Figure S3N).

The NAD+ Precursor Nicotinamide Riboside Rescues Mitochondrial Defects in *GBA*-PD iPSC-Derived Neurons

Next, we tested the ability of different NAD+ precursors to increase NAD+ levels in human iPSC-derived neurons. Control iPSC-derived neurons were treated with nicotinamide (NAM), NMN, or nicotinamide riboside (NR), and NAD+ levels were measured using a NAD+ cycling assay. NR and NMN showed the strongest effect in boosting NAD+ levels (Figure S6A). As NR represents a promising approach, as shown by pharmacokinetic studies in healthy subjects (Trammell et al., 2016), we investigated the ability of NR to rescue *GBA*-linked mitochondrial defects. NR significantly increased NAD+ and NADH levels in *GBA*-PD neurons (Figures S6B and S6C). NR treatment resulted in an increase in expression of markers of mitochondrial biogenesis (TFAM) and mitochondrial UPR (mtUPR) (HSP60) (Figure 5C). Consistent with these findings, mitochondrial DNA content and mitochondrial mass were increased after 48 hr in NR-treated samples (Figures 5D and 5E). The effect of NR was abrogated by EX527, a SIRT1-specific inhibitor, suggesting that SIRT1 is one of the mediators of NR function (Figure S6D). Importantly, NR restored mitochondrial cristae morphology and significantly reduced mtROS production in *GBA*-PD neurons (Figures 5F–5H). In parallel, NR

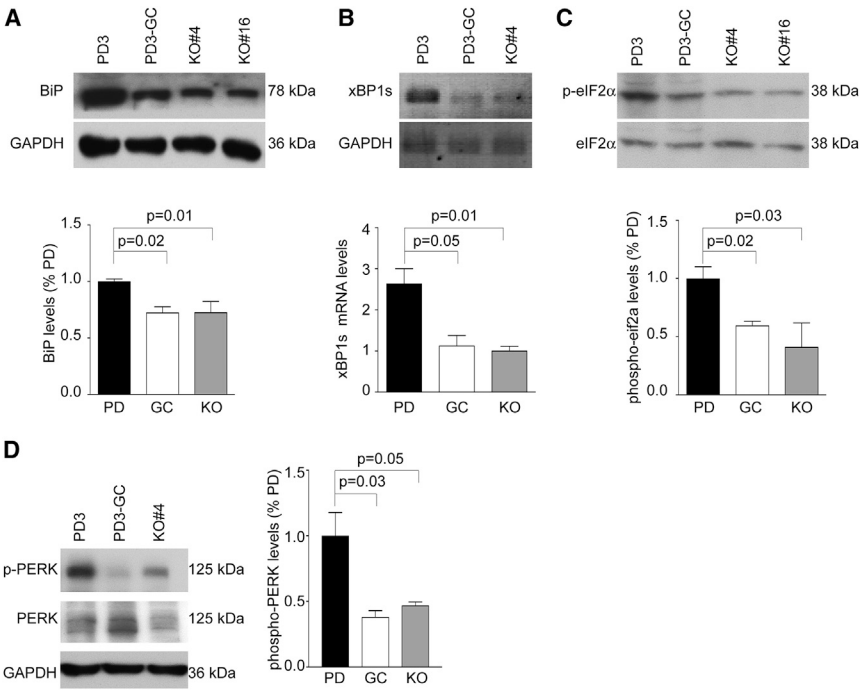

Figure 4. ER Stress Responses in *GBA*-PD and *GBA* KO iPSC Neurons

Analysis of ER stress responses and UPR was performed in isogenic *GBA*-PD (N370S), gene-corrected (GC) controls, and isogenic *GBA* KO (clones 4 and 16) iPSC neurons.

(A) Representative western blots showing BiP levels in isogenic *GBA*-PD, GC, and *GBA* KO iPSC neurons. BiP intensity bands were normalized to GAPDH and the corresponding isogenic control. Data are expressed as mean + SEM (n = 5; one-way ANOVA).

(B) Analysis of XBP1 splicing (XBP1s). mRNA levels of XBP1s were measured by qPCR. Representative agarose gel electrophoresis of qRT-PCR products is shown. For quantification, GAPDH served as reference gene. Data are expressed as mean + SEM (n = 5; one-way ANOVA).

(C) Representative western blots showing phospho-eIF2α/eIF2α levels in isogenic *GBA*-PD, GC, and *GBA* KO iPSC-derived neurons. For quantification, phospho-eIF2α intensity bands were normalized to total eif2α and the corresponding isogenic control. Data are expressed as mean + SEM (one-way ANOVA). Gel loading as in (A).

(D) Representative western blots showing phospho-PERK/PERK levels in isogenic *GBA*-PD, GC, and *GBA* KO iPSC-derived neurons. Data are expressed as mean + SEM (n = 5; one-way ANOVA).

treatment significantly reduced the mitochondrial membrane potential (Figure 5I). Similar results were observed when *GBA* KO neurons were treated with NR (Figures S6E–S6G). With regard to the observed defects in mitochondrial dynamics, NR altered the levels of mitochondrial shaping proteins, with a nonsignificant increase in DRP1, Mfn1, and OPA1 and a slight decrease in Fis1 (Figures 5J and 5K). The decreased levels of mitochondrial DNA content observed at 24 hr after NR treatment would suggest an increased mitochondrial clearance (Figure 5D). In line with these findings, NR was able to increase the levels of BNIP3L/NIX in *GBA*-PD neurons (Figure 5L). NR did not enhance mitochondrial respiration (Figures S6H and S6I). On the contrary, a significant decrease in basal respiration was observed in *GBA*-PD iPSC-derived neurons treated with NR (Figure S6H). In addition, NR treatment did not alter protein levels of BiP in *GBA*-PD neurons (Figure S6J). To confirm that increased NAD+ levels are responsible for the phenotypic rescue, we treated cells with the poly(ADP-ribose)-polymerase (PARP) inhibitor PJ34 that, differently from NAD+ precursors, increases NAD+ levels by inhibiting its consumption. Similar to NR, PJ34 significantly increased NAD+ levels in human-iPSC-derived neurons and rescued mitochondrial defects in *GBA*-PD neurons (Figures S7A–S7E). Taken together, these results suggest that increasing NAD+ levels rescues mitochondrial dysfunction via increased levels of NAD+ in patient-derived *GBA*-PD and *GBA* KO neurons.

Increasing NAD+ Improves Autophagy in *GBA*-PD and *GBA* KO Neurons

GBA mutations affect autophagy and lysosomal function, leading to autophagic block, defects in autophagosome clearance, and altered lysosomal recycling (Schöndorf et al., 2014; Magalhaes et al., 2016). To examine the effects of NR on autophagy, we treated *GBA*-PD and *GBA* KO neurons with NR and assessed parameters of autophagic function. NR treatment did not alter the levels of LC3II at basal conditions; however, it significantly increased LC3II levels in patient neurons treated with leupeptin and ammonium chloride, suggesting an increase of synthesis and clearance of autophagosomes (Figures S7F–S7I). The autophagic flux was significantly increased in *GBA* KO neurons and showed a nonsignificant increase in *GBA*-PD neurons after NR treatment (Figures S7F–S7I).

NR Metabolism and NAD+ Availability in Human iPSC-Derived Neurons

To examine pathways of NAD+ maintenance and NAD+ precursors utilization, control iPSC-derived neurons were treated with the NAMPT inhibitor FK866, and NAD+ levels were measured. FK866 treatment decreased intracellular NAD+ levels by more than 90% (Figure 6A). However, FK866 treatment did not alter the sensitivity of human neurons to NR treatment (Figure 6A), indicating that NR is metabolized into NAD+ in a NAMPT-independent pathway. We next measured the expression levels of the NAD+ biosynthesis enzymes NR kinase 1 and 2 (NRK1 and NRK2) (Bieganowski and Brenner, 2004). In undifferentiated iPSCs, NRK2 showed higher expression levels; on the contrary, levels of NRK1 were significantly higher in iPSC-derived neurons (Figure 6B). The role of NRKs in NAD+ metabolism in human neurons is still unknown. Given its high expression, we aimed to investigate whether NRK1 is essential for NR metabolism into NAD+ in human neurons. Of note, mRNA levels of NRK1 were not affected by NR treatment (Figure 6C). Next, we knocked down NRK1 in control iPSC-derived neurons using

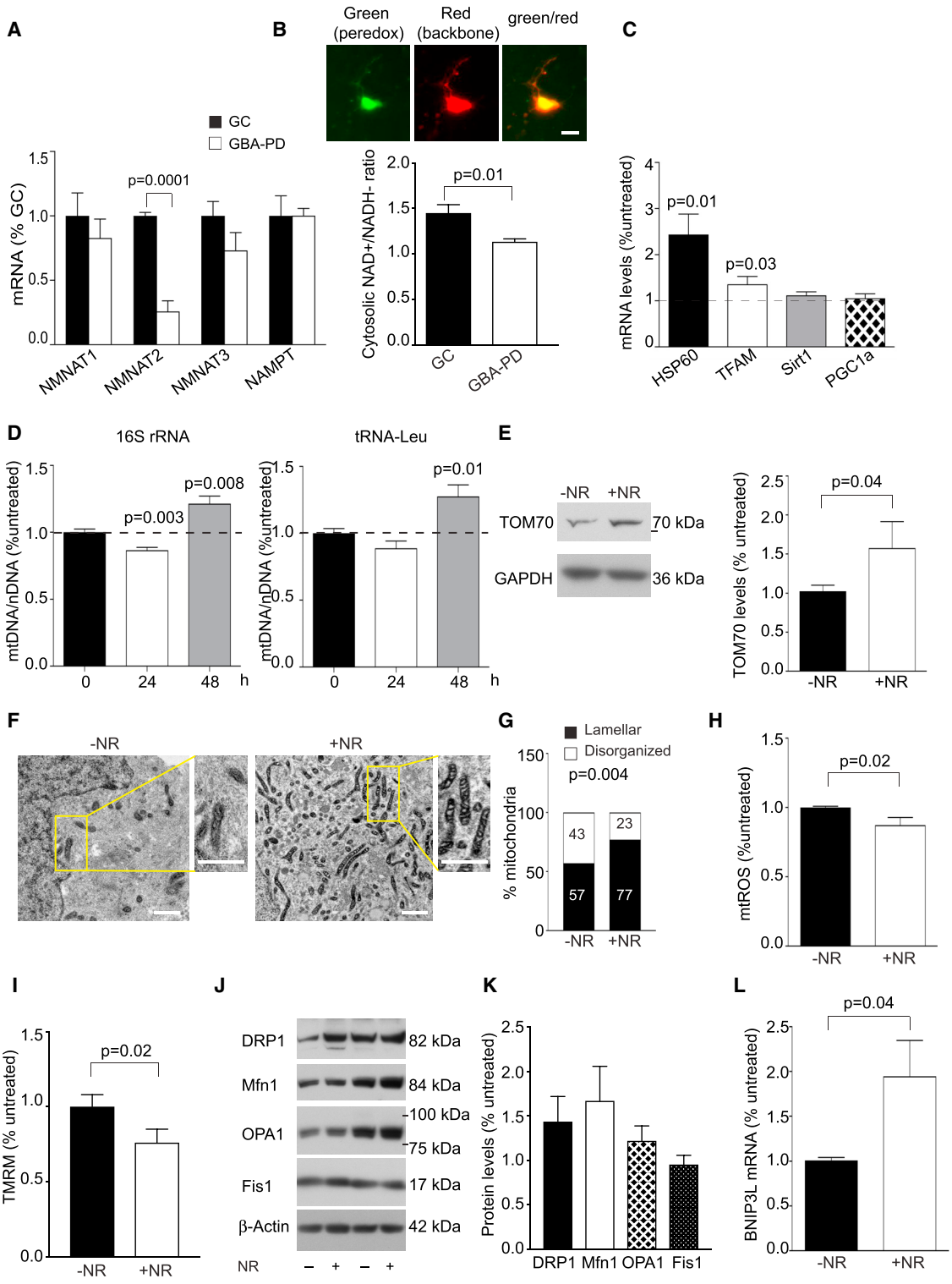

Figure 5. Nicotinamide Riboside Reverts Mitochondrial Defects in *GBA*-PD iPSC Neurons

(A) NMNAT1, NMNAT2, NMNAT3, and NAMPT mRNA levels in isogenic GC and *GBA*-PD (N370S, L444P) iPSC neurons. Data were normalized to the level of the housekeeping genes Rplp0 and OAZ and expressed as fold change over PD. Data are expressed as mean + SEM (n = 5; two-tailed t test).

(B) The NAD+/NADH redox state was measured in iPSC-derived neurons using the biosensor Peredox. Results are presented as mean + SEM (n = 5; two-tailed t test).

(legend continued on next page)

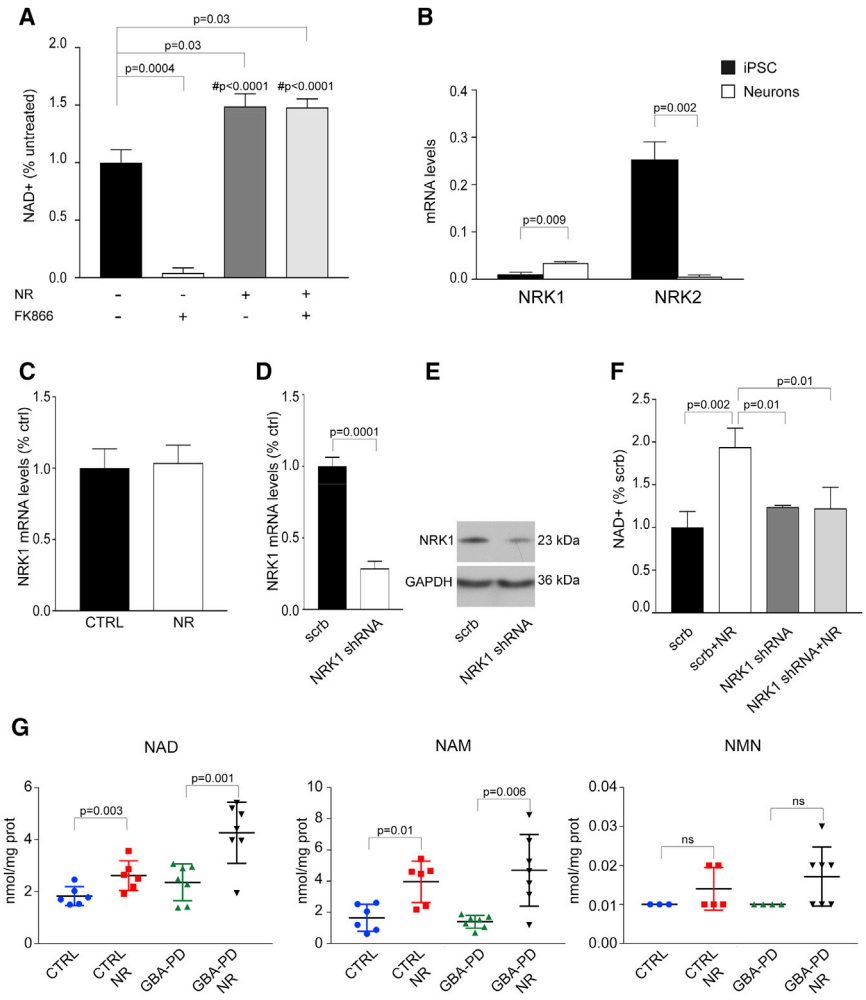

Figure 6. NR Metabolism and Availability in Human iPSC Neurons

(A) Control iPSC neurons were treated with NR with or without the NAMPT inhibitor FK866, and NAD+ levels were measured using a NAD+ cycling assay. Data are expressed as fold changes over untreated neurons and presented as mean + SEM (n = 3; one-way ANOVA). #, significance compared with FK866-treated neurons.

(B) NRK1 and NRK2 mRNA levels were measured in control undifferentiated human iPSCs and iPSC-derived neurons. Data are normalized to Rplp0 levels and expressed as mean + SEM (n = 3; two-tailed t test).

(C) NRK1 mRNA levels were measured in control iPSC neurons with or without NR treatment. Data are normalized to control and presented as mean + SEM (n = 3).

(D) Knockdown efficiency of NRK1 in iPSC neurons was determined by qRT-PCR and normalized to non-targeting shRNA. Data are presented as mean + SEM (n = 3; two-tailed t test).

(E) Representative western blot for NRK1 showing knockdown efficiency in iPSC neurons.

(F) Scramble (Scrb) or NRK1 knockdown control iPSC neurons were treated with NR, and NAD+ levels were measured using a NAD+ cycling assay. Data are expressed as fold changes over untreated and presented as mean + SEM (n = 3; one-way ANOVA).

(G) Control and *GBA*-PD (N370S) iPSC neurons were treated with 0.5 mM NR for 24 hr and LC-MS-based targeted NAD+ metabolomics was performed. Levels of NAD, NAM, and NMN are shown. Data are normalized on protein concentration and presented as mean ± SD (n = 7 independent differentiations; two-tailed t test).

lentiviral-mediated short hairpin RNA (shRNA) (Figures 6D and 6E). NRK1 knockdown did not affect basal levels of NAD+ in neurons, as assessed by a NAD+ cycling assay, whereas NR treatment was unable to significantly increase NAD+ levels in NRK1 knockdown neurons (Figure 6F). These data suggest that NRK1 is essential for exogenous NR metabolism in human neurons. To further examine the metabolism of exogenous NR, we treated control and *GBA*-PD iPSC neurons with 0.5 mM NR and performed LC-MS-based targeted quantitative metabolomics (Figures 6G and S7J). NR treatment significantly increased the levels of NAD+ in control and patient cells. In addition, we found a significant increase of NAM in both groups. On the other

(C) iPSC-derived neurons with *GBA* mutations (N370S and L444P) were treated with NR, and mRNA expression levels of mtUPR and mitochondrial biogenesis markers were measured by qRT-PCR. Data are normalized to untreated and expressed as mean + SEM (n = 5; two-tailed t test).

(D) qRT-PCR was performed to determine mtDNA content as mitochondrial (16S rRNA and tRNA-Leu) to nuclear (β-2M) DNA ratio in untreated samples or after 24- or 48-hr treatment with NR. Data are normalized to untreated and expressed as mean + SEM (n = 5; two-tailed t test).

(E) Western blot showing TOM70 levels. Protein levels are normalized to GAPDH and the corresponding untreated control. Data are presented as mean + SEM (n = 3; two-tailed t test).

(F and G) Mitochondrial morphology was assessed by TEM. Representative TEM images of mitochondria in *GBA*-PD (L444P) iPSC-derived neurons untreated or treated with NR (F; scale bar 500 nm). Quantification of mitochondrial cristae morphology in NR treated and untreated *GBA*-PD iPSC neurons (G; n = 3; two-sided Fisher's exact test).

(H) mtROS in *GBA*-PD (N370S, L444P) iPSC neurons after NR treatment. Data are normalized to the corresponding untreated control and presented as mean + SEM (n = 3; Student's t test).

(I) Mitochondrial membrane potential in *GBA*-PD (N370S, L444P) iPSC neurons after NR treatment. Data are normalized to untreated samples and presented as mean + SEM (n = 5; two-tailed t test).

(J and K) *GBA*-PD (N370S, L444P) iPSC-neurons were treated with NR, and the levels of OPA1, Mfn1, Fis1, and DRP1 were assessed by western blot (J). β-Actin was used as a loading control. Quantification is depicted in (K). Data are represented as mean + SEM (n = 5).

(L) BNIP3L mRNA levels. Data are normalized on Rplp0 and OAZ1 and expressed as fold changes over untreated. Values are presented as mean + SEM (n = 5; Student's t test).

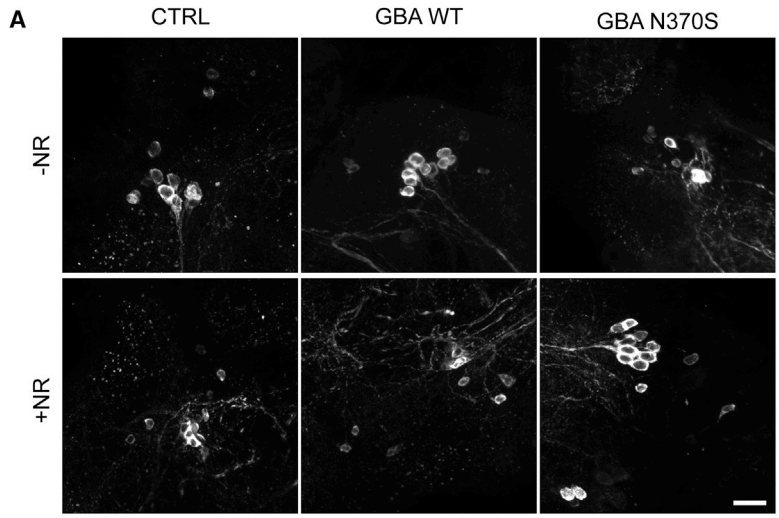

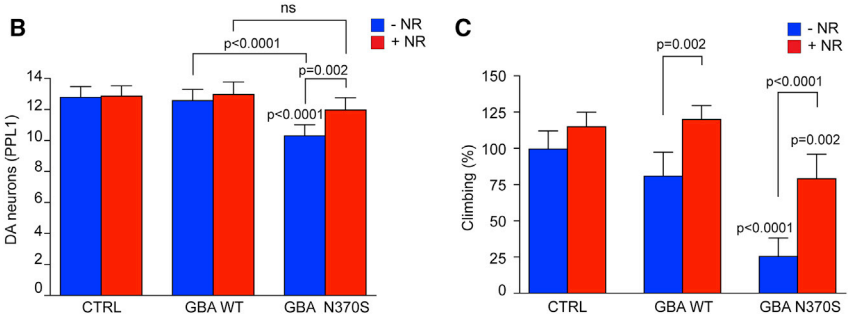

Figure 7. Nicotinamide Riboside Prevents Dopaminergic Neuronal Loss and Rescues Climbing Deficits in *GBA*-PD Flies

(A) Representative confocal images of adult *Drosophila* brains stained with anti-TH antibody. Control and transgenic flies expressing human wild-type (WT) or N370S *GBA* with and without NR treatment (500 μM for 30 days) are shown (scale bar, 10 μm).

(B) Graphs show DA cell counts in absence or presence of NR in PPL1 clusters. Data are presented as mean + SEM (ns, non-significant, n = 8–12 clusters; Kruskal-Wallis with Dunn's multiple comparisons test).

(C) Analysis of climbing ability in adult flies expressing N370S *GBA* variants in the presence or absence of NR (500 μM for 10 days). Data are presented as mean + 95% confidence interval (n = ~50 animals per condition ;Kruskal-Wallis with Dunn's multiple comparisons test).

hand, levels of NMN, the immediate downstream product of NR, tended to be higher in NR-treated cells, but this difference was not statistically significant (Figure 6G).

NR Rescues Motor Deficits in a *Drosophila* Model of *GBA*-PD

To assess the neuroprotective effect of NAD+ precursors *in vivo*, we employed a *Drosophila* model of *GBA*-PD. Flies expressing human N370S *GBA* show increased ER stress, an age-dependent loss of DA neurons accompanied by progressive defects in climbing activity (Sanchez-Martinez et al., 2016). To explore neuroprotection, flies expressing wild-type (WT) or N370S *GBA* were first raised on normal food, and then adult flies were aged on food containing NR (500 μM). At 30 days, expression of N370S *GBA* caused loss of DA neurons in the protocerebral posterial lateral 1 (PPL1) cluster. Strikingly, feeding NR significantly prevented DA neuronal loss compared to untreated controls (Figures 7A and 7B). Importantly, NR treatment also significantly prevented the decline in climbing ability in mutant N370S *GBA* flies (Figure 7C).

DISCUSSION

Mounting evidence suggests that mitochondrial dysfunction plays a key role in PD. Here, we report that neurons from *GBA*-PD patients and *GBA* KO neurons exhibit mitochondrial dysfunction characterized by morphological changes, reduced respiration, and increased oxidative stress. As mitochondrial membrane lipid composition regulates many of these functions (Aufschnaiter et al., 2017) and changes in lipid metabolism have been observed in *GBA*-PD (Schöndorf et al., 2014; Fernandes et al., 2016; García-Sanz et al., 2017), we examined the mitochondrial sphingolipid profile of *GBA*-PD and *GBA* KO neurons. Lipidomic analysis revealed the absence of a significant accumulation of sphingolipids in patient mitochondria. However, we observed a significant increase of C16-GlcCer. On the contrary, the mitochondrial sphingolipid profile of *GBA* KO neurons was profoundly altered, with significant accumulation of GlcCer and glucosylsphingosine. Given the role of sphingolipids in the regulation of mitochondrial properties, substrate accumulation or even subtle changes in lipid composition of mitochondrial membranes, as observed in patient mitochondria, may interfere with their biophysical properties and signaling pathways. However, we are not able to unambiguously define the exact subcellular localization of these alterations. Even though we have isolated mitochondria to the highest degree of purity, a small amount of contamination with lysosomes and ER was still present. The low degree of non-mitochondrial proteins and the complete absence of additional lysosomal markers (other than LAMP1) suggest the residual presence of organelle contact sites in mitochondrial preparations. Given the importance of contact sites in interorganelle communication (Wong et al., 2018), further studies are needed to investigate the role of distinct sphingolipids in such inter-organelle communication and mitochondrial dysfunction.

Overall, we did not observe a gene dosage effect when comparing mitochondrial function in heterozygous *GBA*-PD with *GBA* KO neurons. Thus, distinctly different mechanisms

likely contribute to mitochondrial dysfunction in these models. One such mechanism could be the alteration of mitochondria sphingolipid composition, which we observed in *GBA* KO, but not *GBA*-PD, cells. Interestingly, in other lysosomal storage diseases, the loss of lysosomal enzymatic function leads to substrate accumulation at the ER membranes and subsequent activation of the UPR (Tessitore et al., 2004). However, despite significant substrate accumulation in our model, the complete loss of GCase enzymatic function in *GBA* KO neurons is not sufficient to trigger ER stress responses that were instead observed in heterozygous *GBA*-PD neurons. This points toward a key role of gain-of-function mechanisms in ER stress responses in *GBA*-PD. On the other hand, GCase deficiency results in sphingolipid accumulation and mitochondrial dysfunction including increased mtROS.

GBA-PD neurons showed an imbalance of mitochondrial shaping proteins DRP1, OPA1, Mfn1, and Fis1 and an increased ratio of L-OPA1/S-OPA1. As L-OPA1 processing and impaired DRP1 activity contribute to the dysfunction of mitophagy (MacVicar and Lane, 2014), our results would suggest an impairment of mitochondrial clearance in *GBA*-PD. This was further supported by the reduced mitochondria-lysosome colocalization and reduced expression of the mitophagy adaptor NIX/BNIP3L. Unexpectedly, we did not observe a significant increase of mitochondrial content in patient neurons. The mitochondrial membrane potential was also preserved in *GBA*-PD neurons. As BNIP3L/NIX plays a role in the loss of mitochondrial membrane potential (Sandoval et al., 2008), reduced levels of BNIP3L in *GBA*-PD neurons could explain the lack of decreased mitochondrial membrane potential. Taken together, our data suggest an imbalance of mitochondrial dynamics in *GBA*-PD neurons that leads to mitochondrial dysfunction in the absence of accumulation of damaged mitochondria. As mitophagy occurs locally in distal neuronal axons, we cannot exclude accumulation of dysfunctional mitochondria within axons (Ashrafi et al., 2014).

Increasing intracellular NAD+ concentrations has been shown to be protective against age-related metabolic decline and disease (Rajman et al., 2018; Katsyuba and Auwerx, 2017). NAD+ is a coenzyme for several enzymes, including SIRT1, which regulates mitochondrial biogenesis, autophagy, and cellular stress responses (Chang and Guarente, 2014; Prola et al., 2017). Several mechanisms lead to NAD+ consumption, including oxidative stress. To examine whether NAD+ decline is involved in *GBA*-PD, we have first used targeted metabolomics and found that NAD+ levels were maintained in both *GBA*-PD and *GBA* KO iPSC-derived neurons, as well as whole brains from *gba*$^{-/-}$ zebrafish. As cellular energy metabolism and the cytosolic NADH/NAD+ redox state differ in various tissues or different cells within the same tissue, we have employed a genetically encoded NADH/NAD+ biosensor for live-cell imaging in iPSC-derived neurons. *GBA*-PD neurons showed a significant reduction of the NAD+/NADH redox state. The reduction of NMNAT2 in *GBA*-PD neurons further supports an alteration of NAD+ metabolism in *GBA*-PD. Besides its role in NAD+ synthesis, NMNAT2 also acts as a chaperone to reduce proteotoxic stress and its levels decline prior to the onset of neurodegeneration (Ali et al., 2016). Thus, the reduction of NMNAT2 in *GBA*-PD neurons could also explain the increased proteotoxic stress observed in these cells. The zebrafish metabolomics data further support an alteration of NAD+ metabolism. *GBA* deficiency led to a significant increase in NMN in zebrafish brains. This strongly suggests reduced NMNAT activity in the zebrafish brain when lacking *GBA*. We were unable to reliably detect NMN at basal conditions in iPSC-derived neurons, as NMN is a low abundance metabolite in cellular extracts. In conclusion, even though we cannot yet conclude definitively that NAD+ decline occurs in *GBA*-PD, our data suggest alterations of NAD+ metabolism in these models. Given the existence of different cellular NAD+ pools and the relevance of mitochondrial NAD+ for mitochondrial and cellular function, an important question remains how these NAD+ cellular pools communicate with each other and modulate the aging process and disease risk.

Here, we report that human iPSC-derived neurons rely on NAMPT for maintenance of the NAD+ pool, they are responsive to NAD+ precursors and utilize NRK1 as the main metabolic pathway to synthetize NAD+ from exogenous NR in a NAMPT-independent manner. NR administration caused a significant increase of NAD+. Besides NAD+, levels of NAM were also increased upon NR treatment, suggesting an increase of the activity of NAD+ consuming enzymes that convert NAD+ to NAM. However, we cannot exclude a partial conversion of exogenous NR into NAM before synthesis to NAD+. Levels of the immediate downstream product of NR, NMN, tended to be higher in NR-treated cells, but this difference was not statistically significant. This would suggest a rapid conversion of NMN into NAD+. In our model systems, NR ameliorated mitochondrial function and rescued mitochondrial quality control. We also observed an increased expression of BNIP3L/NIX after NR treatment. In line with this, mitochondrial content decreased after 24 hr of NR treatment, which points toward increased mitophagy. However, prolonged NR treatment boosted mitochondrial content and increased TFAM, which underlines the dual role of NAD+ and sirtuins in maintaining mitochondrial biogenesis and quality control. Furthermore, supporting an increase in mitophagy, NR positively regulated autophagic function. Importantly, we found that NAD+ supplementation rescues the age-dependent loss of DA neurons and decline in motor ability in a *GBA*-PD *Drosophila* model.

In summary, our study elucidates the mechanisms involved in *GBA*-PD and reveals mitochondrial dysfunction as a key driver of disease. Our findings show that NAD+ precursors ameliorate *GBA*-related defects. Among the available NAD+ precursors, NR may be a valuable therapeutic approach due to its high bioavailability, minimal toxicity, and evidence of its ability to cross the blood-brain barrier (Trammell et al., 2016). Future studies will explore the potential therapeutic benefits of combining NAD+ boosters with chaperones and GCase activators (Migdalska-Richards et al., 2016).

EXPERIMENTAL PROCEDURES

Cell Culture

iPSC lines (Table S1) were previously generated and characterized (Schöndorf et al., 2014).

Generation of *GBA* Knockout Human iPSCs

CRISPR-Cas9 constructs were generated as described previously (Ran et al., 2013).

Measurement of Mitochondrial Membrane Potential and mtROS

Neurons were washed once with Hank's balanced salt solution (HBSS) (Invitrogen) following incubation with 200 nM tetramethylrhodamine methylester perchlorat (TMRM) (Invitrogen). For measurements of mtROS, cells were incubated with 5 μM MitoSOX Red (Invitrogen). Cytofluorimetric analysis was performed using MACSQuant Analyzer 10 (Miltenyi).

Seahorse XF^{e}96 Metabolic Flux Analysis

OCR was analyzed using an XF^{e}96 Extracellular Flux Analyzer (Seahorse Biosciences).

NAD/NADH Measurements and Metabolomics

NAD+ levels were measured using the NAD/NADH-Glo Assay Kit (Promega). NADH levels were measured using the NAD/NADH Assay Kit (Abcam). The cytosolic NADH/NAD+ redox state of iPSC neurons was measured as described previously (Hung et al., 2011).

Enzymatic Activities

GCase activity was tested using the intact cell lysosomal β-Glu assay (Sawkar et al., 2006). Citrate synthase and mitochondrial CI activities were measured following the protocol reported by Spinazzi et al. (2012).

Drosophila Studies

Transgenic *Drosophila* lines expressing human WT or N370S *GBA* were previously generated (Sanchez-Martinez et al., 2016).

Statistical Analysis

The Statistical Package GraphPad Prism version 7.0b (GraphPad Software, San Diego, CA) was used to analyze the data. Statistical testing involved a two-sided Fisher's exact test, two-tailed Student's t test, one-way ANOVA with Bonferroni's multiple comparison test, or Kruskal-Wallis with Dunn's multiple comparisons test, as appropriate. Data are expressed as mean + SEM or SD as indicated.

SUPPLEMENTAL INFORMATION

Supplemental Information includes Supplemental Experimental Procedures, seven figures, and two tables and can be found with this article online at https://doi.org/10.1016/j.celrep.2018.05.009.

ACKNOWLEDGMENTS

We are grateful to Katharina Demandt, Ulrike Ulmer, Selina Reich, and Maria Zarani for their excellent experimental help and Simone Pöschel from the Imaging Flow Cytometry Core Facility, University of Tübingen for excellent assistance with the Amnis ImageStream. This work was made possible through funding by the German Research Council (DFG; DE 2157/2-1; M.D.), Helmholtz Association (VH-NG-1123; M.D.), Marie Curie Career Integration Grant (CIG304108; M.D.), Medical Research Council core funding (MC-A070-5PSB0; A.J.W.), and the European Research Council (starting grant 309742; AJW). Research was supported in part by the Medical University of South Carolina's Lipidomics Shared Resource through funding of laboratory space for the Analytical Unit located in 505 Children's Research Institute (CRI): Hollings Cancer Center (P30 CA138313), the Lipidomics Shared Resource in the South Carolina Lipidomics and Pathobiology COBRE; MUSC Department of Biochemistry (P20 RR017677), and the National Center for Research Resources and Office of the Director of the National Institutes of Health (C06 RR018823)

AUTHOR CONTRIBUTIONS

M.D. conceived, designed, and supervised the study. A.J.W. designed *Drosophila* studies. D.C.S., D.I., P.B., S.D.C., C.Y., L.K.S., G.D.N., V.P., and J.P. performed *in vitro* experiments. D.C.S., D.I., P.B., S.D.C., and L.K.S. analyzed data. S.N. and B.H. performed TEM, A.S.-M. and I.G. performed *Drosophila* studies and analyzed data, and M.K. and O.B. performed zebrafish experiments. T.G. oversaw patient sample collection. M.D. wrote the manuscript with input from all authors. All authors contributed to proofreading of the manuscript.

DECLARATION OF INTERESTS

The authors declare no competing interests.

Received: September 7, 2017
Revised: March 5, 2018
Accepted: May 2, 2018
Published: June 5, 2018

REFERENCES

Ali, Y.O., Allen, H.M., Yu, L., Li-Kroeger, D., Bakhshizadehmahmoudi, D., Hatcher, A., McCabe, C., Xu, J., Bjorklund, N., Taglialatela, G., et al. (2016). NMNAT2:HSP90 complex mediates proteostasis in proteinopathies. PLoS Biol. *14*, e1002472.

Ashrafi, G., Schlehe, J.S., LaVoie, M.J., and Schwarz, T.L. (2014). Mitophagy of damaged mitochondria occurs locally in distal neuronal axons and requires PINK1 and Parkin. J. Cell Biol. *206*, 655–670.

Aufschnaiter, A., Kohler, V., Diessl, J., Peselj, C., Carmona-Gutierrez, D., Keller, W., and Büttner, S. (2017). Mitochondrial lipids in neurodegeneration. Cell Tissue Res. *367*, 125–140.

Bieganowski, P., and Brenner, C. (2004). Discoveries of nicotinamide riboside as a nutrient and conserved NRK genes establish a Preiss-Handler independent route to NAD+ in fungi and humans. Cell *117*, 495–502.

Chang, H.C., and Guarente, L. (2014). SIRT1 and other sirtuins in metabolism. Trends Endocrinol. Metab. *25*, 138–145.

Cleeter, M.W., Chau, K.Y., Gluck, C., Mehta, A., Hughes, D.A., Duchen, M., Wood, N.W., Hardy, J., Mark Cooper, J., and Schapira, A.H. (2013). Glucocerebrosidase inhibition causes mitochondrial dysfunction and free radical damage. Neurochem. Int. *62*, 1–7.

Exner, N., Lutz, A.K., Haass, C., and Winklhofer, K.F. (2012). Mitochondrial dysfunction in Parkinson's disease: molecular mechanisms and pathophysiological consequences. EMBO J. *31*, 3038–3062.

Fernandes, H.J., Hartfield, E.M., Christian, H.C., Emmanoulidou, E., Zheng, Y., Booth, H., Bogetofte, H., Lang, C., Ryan, B.J., Sardi, S.P., et al. (2016). ER stress and autophagic perturbations lead to elevated extracellular α-synuclein in GBA-N370S Parkinson's iPSC-derived dopamine neurons. Stem Cell Reports *6*, 342–356.

García-Sanz, P., Orgaz, L., Bueno-Gil, G., Espadas, I., Rodríguez-Traver, E., Kulisevsky, J., Gutierrez, A., Dávila, J.C., González-Polo, R.A., Fuentes, J.M., et al. (2017). N370S-GBA1 mutation causes lysosomal cholesterol accumulation in Parkinson's disease. Mov. Disord. *32*, 1409–1422.

Gegg, M.E., Burke, D., Heales, S.J., Cooper, J.M., Hardy, J., Wood, N.W., and Schapira, A.H. (2012). Glucocerebrosidase deficiency in substantia nigra of Parkinson disease brains. Ann. Neurol. *72*, 455–463.

Hung, Y.P., Albeck, J.G., Tantama, M., and Yellen, G. (2011). Imaging cytosolic NADH-NAD(+) redox state with a genetically encoded fluorescent biosensor. Cell Metab. *14*, 545–554.

Jansen, I.E., Ye, H., Heetveld, S., Lechler, M.C., Michels, H., Seinstra, R.I., Lubbe, S.J., Drouet, V., Lesage, S., Majounie, E., et al.; International Parkinson's Disease Genetics Consortium (IPGDC) (2017). Discovery and functional prioritization of Parkinson's disease candidate genes from large-scale whole exome sequencing. Genome Biol. *18*, 22.

Jo, E., McLaurin, J., Yip, C.M., St George-Hyslop, P., and Fraser, P.E. (2000). alpha-Synuclein membrane interactions and lipid specificity. J. Biol. Chem. *275*, 34328–34334.

Katsyuba, E., and Auwerx, J. (2017). Modulating NAD$^+$ metabolism, from bench to bedside. EMBO J. *36*, 2670–2683.

Keatinge, M., Bui, H., Menke, A., Chen, Y.C., Sokol, A.M., Bai, Q., Ellett, F., Da Costa, M., Burke, D., Gegg, M., et al. (2015). Glucocerebrosidase 1 deficient

Danio rerio mirror key pathological aspects of human Gaucher disease and provide evidence of early microglial activation preceding alpha-synuclein-independent neuronal cell death. Hum. Mol. Genet. *24*, 6640–6652.

MacVicar, T.D., and Lane, J.D. (2014). Impaired OMA1-dependent cleavage of OPA1 and reduced DRP1 fission activity combine to prevent mitophagy in cells that are dependent on oxidative phosphorylation. J. Cell Sci. *127*, 2313–2325.

Magalhaes, J., Gegg, M.E., Migdalska-Richards, A., Doherty, M.K., Whitfield, P.D., and Schapira, A.H. (2016). Autophagic lysosome reformation dysfunction in glucocerebrosidase deficient cells: relevance to Parkinson disease. Hum. Mol. Genet. *25*, 3432–3445.

Maor, G., Rencus-Lazar, S., Filocamo, M., Steller, H., Segal, D., and Horowitz, M. (2013). Unfolded protein response in Gaucher disease: from human to Drosophila. Orphanet J. Rare Dis. *8*, 140.

Mazzulli, J.R., Xu, Y.H., Sun, Y., Knight, A.L., McLean, P.J., Caldwell, G.A., Sidransky, E., Grabowski, G.A., and Krainc, D. (2011). Gaucher disease glucocerebrosidase and α-synuclein form a bidirectional pathogenic loop in synucleinopathies. Cell *146*, 37–52.

Migdalska-Richards, A., and Schapira, A.H. (2016). The relationship between glucocerebrosidase mutations and Parkinson disease. J. Neurochem. *139* (*Suppl 1*), 77–90.

Migdalska-Richards, A., Daly, L., Bezard, E., and Schapira, A.H. (2016). Ambroxol effects in glucocerebrosidase and α-synuclein transgenic mice. Ann. Neurol. *80*, 766–775.

Mouchiroud, L., Houtkooper, R.H., Moullan, N., Katsyuba, E., Ryu, D., Cantó, C., Mottis, A., Jo, Y.S., Viswanathan, M., Schoonjans, K., et al. (2013). The NAD(+)/sirtuin pathway modulates longevity through activation of mitochondrial UPR and FOXO signaling. Cell *154*, 430–441.

Osellame, L.D., Rahim, A.A., Hargreaves, I.P., Gegg, M.E., Richard-Londt, A., Brandner, S., Waddington, S.N., Schapira, A.H., and Duchen, M.R. (2013). Mitochondria and quality control defects in a mouse model of Gaucher disease: links to Parkinson's disease. Cell Metab. *17*, 941–953.

Prola, A., Pires Da Silva, J., Guilbert, A., Lecru, L., Piquereau, J., Ribeiro, M., Mateo, P., Gressette, M., Fortin, D., Boursier, C., et al. (2017). SIRT1 protects the heart from ER stress-induced cell death through eIF2α deacetylation. Cell Death Differ. *24*, 343–356.

Rajman, L., Chwalek, K., and Sinclair, D.A. (2018). Therapeutic potential of NAD-boosting molecules: the in vivo evidence. Cell Metab. *27*, 529–547.

Ran, F.A., Hsu, P.D., Wright, J., Agarwala, V., Scott, D.A., and Zhang, F. (2013). Genome engineering using the CRISPR-Cas9 system. Nat. Protoc. *8*, 2281–2308.

Rocha, E.M., Smith, G.A., Park, E., Cao, H., Brown, E., Hallett, P., and Isacson, O. (2015). Progressive decline of glucocerebrosidase in aging and Parkinson's disease. Ann. Clin. Transl. Neurol. *2*, 433–438.

Sanchez-Martinez, A., Beavan, M., Gegg, M.E., Chau, K.Y., Whitworth, A.J., and Schapira, A.H. (2016). Parkinson disease-linked GBA mutation effects reversed by molecular chaperones in human cell and fly models. Sci. Rep. *6*, 31380.

Sandoval, H., Thiagarajan, P., Dasgupta, S.K., Schumacher, A., Prchal, J.T., Chen, M., and Wang, J. (2008). Essential role for Nix in autophagic maturation of erythroid cells. Nature *454*, 232–235.

Sawkar, A.R., Schmitz, M., Zimmer, K.P., Reczek, D., Edmunds, T., Balch, W.E., and Kelly, J.W. (2006). Chemical chaperones and permissive temperatures alter localization of Gaucher disease associated glucocerebrosidase variants. ACS Chem. Biol. *1*, 235–251.

Schapira, A.H., Cooper, J.M., Dexter, D., Jenner, P., Clark, J.B., and Marsden, C.D. (1989). Mitochondrial complex I deficiency in Parkinson's disease. Lancet *1*, 1269.

Schöndorf, D.C., Aureli, M., McAllister, F.E., Hindley, C.J., Mayer, F., Schmid, B., Sardi, S.P., Valsecchi, M., Hoffmann, S., Schwarz, L.K., et al. (2014). iPSC-derived neurons from GBA1-associated Parkinson's disease patients show autophagic defects and impaired calcium homeostasis. Nat. Commun. *5*, 4028.

Sidransky, E., Nalls, M.A., Aasly, J.O., Aharon-Peretz, J., Annesi, G., Barbosa, E.R., Bar-Shira, A., Berg, D., Bras, J., Brice, A., et al. (2009). Multicenter analysis of glucocerebrosidase mutations in Parkinson's disease. N. Engl. J. Med. *361*, 1651–1661.

Spinazzi, M., Casarin, A., Pertegato, V., Salviati, L., and Angelini, C. (2012). Assessment of mitochondrial respiratory chain enzymatic activities on tissues and cultured cells. Nat. Protoc. *7*, 1235–1246.

Tessitore, A., del P Martin, M., Sano, R., Ma, Y., Mann, L., Ingrassia, A., Laywell, E.D., Steindler, D.A., Hendershot, L.M., and d'Azzo, A. (2004). GM1-ganglioside-mediated activation of the unfolded protein response causes neuronal death in a neurodegenerative gangliosidosis. Mol. Cell *15*, 753–766.

Trammell, S.A., Schmidt, M.S., Weidemann, B.J., Redpath, P., Jaksch, F., Dellinger, R.W., Li, Z., Abel, E.D., Migaud, M.E., and Brenner, C. (2016). Nicotinamide riboside is uniquely and orally bioavailable in mice and humans. Nat. Commun. *7*, 12948.

Velayati, A., Yu, W.H., and Sidransky, E. (2010). The role of glucocerebrosidase mutations in Parkinson disease and Lewy body disorders. Curr. Neurol. Neurosci. Rep. *10*, 190–198.

Wong, Y.C., Ysselstein, D., and Krainc, D. (2018). Mitochondria-lysosome contacts regulate mitochondrial fission via RAB7 GTP hydrolysis. Nature *554*, 382–386.